PFC/JA-94-027

Thermal Front Analysis of Detached Divertors and Marfes

I.H. Hutchinson

Plasma Fusion Center
Massachusetts Institute of Technology
Cambridge, MA 02139

September 1994

Submitted to Nuclear Fusion.

This work was supported by the U. S. Department of Energy Contract No. DE-AC02-78ET51013. Reproduction, translation, publication, use and disposal, in whole or in part by or for the United States government is permitted.

Thermal Front Analysis of Detached Divertors and Marfes

I.H.Hutchinson

Plasma Fusion Center

Massachusetts Institute of Technology

Cambridge, Massachusetts, USA

Abstract

Nonlinear analysis is presented of localized regions of strong divergence of parallel heat flux — thermal fronts — in the edge and scrape-off-layer of tokamaks. The phenomena of divertor detachment and marfes are discussed in terms of one-dimensional thermal conduction in the parallel coordinate, but retaining cross-field transport power divergence and radiation as source terms. Full finite aspect-ratio geometry is retained and has important effects. Thermal fronts are shown to require either localization of the source terms or density control, to be stable against parallel motion. The edge density range over which the front is naturally localized to the divertor leg is shown to be rather small. The size, stability, and preferred position of marfes are predicted and are in agreement with experiment.

1. Introduction

The behaviour of radiative regions in the edge of tokamaks has attracted considerable attention, especially since the "dissipative divertor" has become the preferred solution for reducing ITER's divertor-plate heat loads. Experimental observations of detached divertor operation [1,2,3] have been made in several tokamaks. These operating modes have documented substantial plasma energy flux reductions as a result of radiative losses leading apparently to large heat flux gradients parallel to the magnetic field. It is important to distiguish between "detached divertor" operation, in which the power is suppressed at the divertor plates but the main scrape-off-layer remains hot, from "detached plasma" operation, seen also in limiter discharges, where the plasma edge is cold all around the poloidal circumference and parallel heat flux gradients are not significant. Detached divertor operation is our present concern.

A closely related phenomenon is the marfe [4,5,6]: a localized radiative region in the plasma edge that is axisymmetric and hence has substantial parallel gradients of temperature, density and heat flow. Indeed, in some cases, the divertor detachment appears to be related to the formation of a marfe-like region near the magnetic x-point.

Large, two-dimensional, multifluid, computer simulations of detached divertor and marfe behaviour have been vigorously pursued [7,8], and various suggestive phenomena have been observed in these numerical experiments, e.g. [9]. The large codes have the merit of rather realistic geometry, and the ability to follow the atomic physics of hydrogenic species in considerable detail (e.g. [10]). However, since (among other limitations) the perpendicular transport coefficients and their spatial and parametric dependences are essentially unknown, the boundary conditions applied to the simulational region are rather *ad hoc*, and the impurity species modelling is at a rudimentary stage, it is clear that the details of such simulations should be treated with caution. Moreover, with so many free parameters and such complex nonlinear behaviour, even if the simulations were definitive and gave good agreement with experiments, it would still be necessary to *interpret* those simulations. That is, the results would have to be analysed and organized using compound concepts such as flow reversal, thermal or ionization fronts, neutral cushions, and so on, before a true understanding of the factors governing the divertor behaviour could be claimed and sufficient confidence in future designs obtained.

The purpose of this paper is to study the theoretical behaviour of thermal fronts: that is, localized regions of parallel heat flux gradient. It is shown that several characteristic nonlinear features of such fronts can be understood analytically and used to discuss the general behaviour of radiative divertors and marfes. The dominant processes in such fronts are parallel heat flow divergence balanced against radiative losses. Therefore it is appropriate to consider only one dimension, along the field, approximating perpendicular flux divergences as sources in the one-dimensional equation. Although this approximation excludes much complex two-dimensional behaviour, one-dimensional treatments give much insight, and have often proven to be quantitatively quite accurate [11]. Also, when the perpendicular transport coefficients are so uncertain, any accuracy lost in the one-dimensional approach may be equally elusive in two-dimensional simulations.

The present approach focusses on the energy equation, since heat flow is our interest. The momentum equation is treated approximately via a constraint of constant pressure, and the continuity equation is treated only indirectly by assumptions about the average density variation. The justification for this is the demonstration that there are characteristics of the energy equation's behaviour that can be understood separately from the other complexities. Where necessary, it must be understood that we are assuming that the continuity and momentum equations can be satisfied by some unspecified processes. This assumption is most likely to be reasonable when we are discussing the high-density, collisional, conduction-limited scrape off layer (SOL), which is the regime most likely to exhibit thermal fronts: divertor detachment and marfes.

The analysis is in some respects related to previous discussions of marfe stability on the basis of heat conduction equations [12,13,14]. However, it is different in several respects. First, unlike the analysis of Drake, [13], we focus on the parallel conduction, not the perpendicular. Second, these earlier analytical treatments are linear stability analyses of poloidally uniform equilibria. In contrast, the present concern is the non-linear behaviour of already formed radiative non-uniformities, their size, position, stability, interaction with divertor boundaries, and general characteristics. Third, we retain as far as possible a general treatment of the radiation form (as distinct from the very specific nonlinear solution of [15]). And finally we treat the geometry in a general way that accounts for such aspects of the fluxes as finite aspect-ratio effects

and poloidal field variation along the surface.

Recent work of Capes *et al.* [16] discussed edge temperature bifurcation. The present work goes substantially further in that it investigates directly the formation of localized fronts, and addresses the realistic case where transverse heat flux divergence is important.

2. Formulation

We consider a situation in which heat transport can be taken as purely conductive, with convection ignored for simplicity. We use natural, flux-surface, coordinates: toroidal angle ϕ with associated unit vector $\mathbf{e}_\phi$, poloidal flux, ψ such that the poloidal field is $\mathbf{B}_p = \mathbf{e}_\phi \wedge \nabla\psi/R$, and poloidal arc length l_p. The heat balance equation for an axisymmetric case can then be written

$$\frac{|\nabla\psi|}{R}\nabla_p\left(\frac{R}{|\nabla\psi|}q_p\right) = B_p\frac{\partial}{\partial l_p}\left(\frac{1}{B_p}\kappa_p\frac{\partial}{\partial l_p}T\right) = -H \quad , \tag{1}$$

where subscript p means the poloidal direction along the flux surface and H is the sum of volumetric power source density plus the contribution from the divergence of heat flow across flux surfaces: $\kappa_\psi\nabla_\psi T$. Note that $\delta\psi R/|\nabla\psi| = \delta\psi/B_p$ is the area across which the poloidal heat flux flows, between two flux surfaces separated by $\delta\psi$,

The poloidal heat conduction, $q_p = \kappa_p\partial T/\partial l_p$, can be expressed in terms of components parallel and perpendicular to the field: $q_\| = \kappa_\|\nabla_\| T$, and $q_\wedge = \kappa_\wedge\nabla_\wedge T$, where $\nabla_\| \equiv (1/B)\mathbf{B}_p.\nabla$, and $\nabla_\wedge \equiv (\mathbf{B}\wedge\nabla\psi/B|\nabla\psi|).\nabla = (B_\phi/BB_p)\mathbf{B}_p.\nabla$. Then, since $q_p = (B_p/B)q_\| + (B_\phi/B)q_\wedge$, the poloidal conductivity can immediately be written

$$\kappa_p = \frac{B_p^2}{B^2}\kappa_\| + \frac{B_\phi^2}{B^2}\kappa_\wedge \quad . \tag{2}$$

Eq.(1) can be reexpressed by transforming to a parallel coordinate z, such that $B_p dz = B_0 dl_p$, where B_0 is a (fixed) typical total field. We find

$$\frac{\partial}{\partial z}\left(\kappa\frac{\partial T}{\partial z}\right) = -H \quad , \tag{3}$$

where

$$\kappa \equiv \kappa_p\frac{B_0^2}{B_p^2} = \frac{B_0^2}{B^2}\kappa_\| + \frac{B_\phi^2 B_0^2}{B_p^2 B^2}\kappa_\wedge \tag{4}$$

is the effective parallel conductivity. This is a more natural coordinate system for the case where κ is dominated by parallel conduction. Eq. (3) refers physically to conduction along a 'flux tube' whose cross-sectional area is inversely proportional to the

total field, B. We see that the effective parallel conductivity is actually approximately inversely proportional to B^2. (An alternative is to use the true parallel distance l such that $B_p dl = B dl_p$, but that leads to a less convenient mathematical form, where the spatial variation of B appears outside the derivative: $(B/B_0)\partial/\partial l[(\kappa B/B_0)\partial T/\partial l] = -H$.) The deceptively simple-looking Eq.(3) is the basis of our one-dimensional investigation. The functional dependencies of κ and H determine the characteristics of its solution.

Normally, the $\nabla_\wedge$ term is ignored on the grounds that the parallel conductivity is so much larger than the perpendicular. The relative importance of this term may be estimated by approximating the derivatives as scale-lengths: $\nabla_\perp \sim 1/\lambda_\perp$ $\nabla_p \sim 1/L_p$. Then, equating the parallel conducted power to the perpendicular divergence, we get $\kappa_\| \nabla_\| T \sim (L/2)\kappa_\perp T/\lambda_\perp^2$, so that

$$\frac{\nabla_\wedge \kappa_\wedge \nabla_\wedge T}{\nabla_\| \kappa_\| \nabla_\| T} \sim \frac{B_\phi}{B_p}\frac{\kappa_\wedge}{\kappa_\perp}\frac{\lambda_\perp^2}{L L_p} \quad . \tag{5}$$

For a localized front, the poloidal scale length may under extreme circumstances be as short as the SOL thickness $L_p \sim \lambda_\perp$. The ratio $\kappa_\wedge/\kappa_\perp$ depends on the anomalous diffusivity due to turbulence, but assuming that this dominates over classical perpendicular transport, it is reasonable to assume that the ratio is of order unity. Since the SOL length, L, is perhaps 1000 times $\lambda_\perp$, the ratio of the power divergence terms is unity only when $B_p/B_\phi \sim \lambda_\perp/L \sim 1/1000$. Thus the $\nabla_\wedge$ term can be significant only where the poloidal field is very much less than its typical value of $\sim B_\phi/10$; that is, only very near the x-point. The effective conductivity, κ, is increased there but only significantly in an extremely small region where B_p is small enough. We shall be well justified in retaining only the $\kappa_\|$ term in most situations. If we had done so from the beginning, Eq. (3) could have been derived directly from the expression for the divergence of parallel flux: $\nabla.[\kappa_\|(\mathbf{B}/B)(\mathbf{B}/B).\nabla T)] = B d/dl[(\kappa_\|/B) dT/dl]$, regardless of axisymmetry.

The contributions to H are perpendicular transport from the adjacent flux surfaces, denoted S, and radiative losses, denoted R. Thus $H = S - R$. We shall ignore the possibility of internal heating or any distinction between electron and ion temperatures for simplicity. In general, H is a function of T and z, and depends on many details of the radiative species and processes. However, at any position, the general form of H as a function of temperature will be as illustrated in Figure 1. At low temperature the heating will be small and non-negative (since cooling at $T = 0$ is physically impossible).

As the temperature rises, R rises, and so H passes through zero at a temperature $T_c \geq 0$. As R rises further it then tends to dominate the heating term but eventually the radiation falls off, because of the ionization of the more radiative atomic states. Consequently, H has a minimum at a large negative value. Radiation finally becomes essentially negligible compared to the transport term at a temperature T_h.

In the presence of such a heating term, one can envisage the occurrence of a thermal front of the form illustrated in Figure 2. Here the solution to Eq. (3) can be considered to consist of 3 regions. The first is the cold region, in which the temperature is flat at a value of essentially T_c. (Note that if H is not explicitly dependent on z then with appropriate boundary conditions, $T = const. = T_c$ is a solution to Eq. (3).) The second region is the thermal front, in which the dominant radiation loss takes place; the temperature rises from T_c to T_h. In the third, hot, region, the radiation is negligible compared to the transport and the temperature rises, but with a negative second derivative. The question we wish to address is whether the thermal front solution is stable. That is, supposing such an equilibrium solution to exist, will it remain in steady state or will the front tend to move either to the right or to the left to a new state.

Initially we will consider the boundary conditions on the solution to be that the temperature is held at a fixed value $T(0) = T_c$. This takes credit for the prior realization that if a detached solution is in fact to be obtained, then the approximately uniform solution in the cold region must be near T_c. More complicated boundary conditions based on sheath conditions are possible but have little impact on the conclusions. The right-hand boundary condition will be considered initially to be a symmetry condition: $dT/dz = 0$ at $z = L$ where L is the (half) length of the SOL to the stagnation point.

We require some assumptions about the dependence of S on T. This somewhat debatable question arises for all SOL analysis, including the boundary conditions of two-dimensional simulations. In the situation where the total power flowing out into the SOL is prescribed, a natural assumption is to take S independent of T. In other words, the heat flow into the SOL is prescribed constant (not necessarily uniform) at all positions and temperatures. Another natural possibility, when we are considering only part of the SOL $\delta\psi$ with adjacent surfaces at effectively constant temperature, is to take $S \propto T_s - T$.

We can express the radiation in the form $R = n_e n_I Q(T) = n^2 f_I Q(T)$ where $n_e = n$ is the electron density, $n_I \equiv n f_I$ is the density of the radiating atomic species, and $Q(T)$ is the radiation function, to first order independent of n. The pressure is generally approximately constant along a flux surface (ignoring the momentum convection term from the pressure balance, consistent with ignoring thermal convection.) It is natural then to write the radiation in terms of the pressure, $p = nT$

$$R = f_I p^2 Q(T)/T^2 \quad . \tag{6}$$

Figure 1 will be regarded as a plot of R at constant pressure ($\propto Q(T)/T^2$) so that we can apply it to a uniform plasma flux surface on which p is constant.

3. Uniform Source-Functions

We multiply Eq (3) by $\kappa dT/dz$ and integrate across the thermal front, i.e. from $z = z_c$ (the rightmost position where $T = T_c$) to $z = z_h$ (where $T = T_h$) to obtain

$$\left(\kappa \frac{dT}{dz}\right)_h^2 - \left(\kappa \frac{dT}{dz}\right)_c^2 = \int_{T_c}^{T_h} -2\kappa H dT. \tag{7}$$

Naturally, for a detached solution we require the heat flow to be zero at the left hand end of the front (z_c), in which case the second term in Eq. (7) is zero. Thus the slope of a detached solution at the boundary between the hot region and the thermal front is given by the integral over the front of κH, and in particular the heat flow at the hot end of the front is given by

$$q_f = -\left(\kappa \frac{dT}{dz}\right)_h = -\sqrt{\int_{T_c}^{T_h} -2\kappa H dT} \quad . \tag{8}$$

It should be noted that the form of this first integral of the conduction equation is independent of the choice of coordinate system.

Returning to Eq. (3) and integrating from z_h to L, i.e. over the hot inner region, we find

$$q_i = -\kappa \left(\frac{dT}{dz}\right)_h = -\int_{z_h}^{L} H \, dz \quad . \tag{9}$$

We can regard q_f and q_i as unique functions of the front position, z_h. The equilibrium requires that the heat flow from the thermal front integration, Eq. (8), and from the inner hot region integration, Eq. (9), should match at the join of the two regions:

$$q_i = q_f \quad . \tag{10}$$

In a non-equilibrium situation, the front will move. The direction of motion depends on the sign of $q_i - q_f$. If the dissipation in the front, $-q_f$, is less than the total heat input to the SOL, $-q_i$, then there is a net heat input into the SOL and its temperature will rise. This implies that the front moves towards the cold side (smaller z), because the front position, z_h, is the point at which the temperature has the fixed value T_h. If the heat imbalance is the opposite, $q_i - q_f > 0$, then the front will move toward the hot side (greater z). (From the viewpoint of a stability analysis linearized about the an original front equilibrium, this simple conclusion requires the eigenmode of interest to be unipolar, i.e. have no zero crossings, which is the case for the most unstable mode.)

The stability of the solution then depends on the derivatives of the two fluxes with respect to the position of the front. Stability requires that

$$\frac{d}{dz_h}(q_i - q_f) \leq 0 \quad , \tag{11}$$

at the equilibrium point where $q_i = q_f$.

If κ and H are not explicit functions of position, but only functions of temperature, then the integrand in Eq. (8) is a unique function of temperature, and so q_f is a constant, independent of z_h. Meanwhile, from Eq. (9), $dq_i/dz_h = H(z_h)$, which is positive since $\int H dz$ is positive and H is uniform. Therefore the stability criterion, Eq. (11) is always violated and a detached thermal front in a SOL whose source terms are not explicitly dependent on position is always positionally unstable.

If the radiation term, R is raised from an initially low value, then the solution develops a decreasing slope at the boundary. However, as soon as the slope reaches zero, and the heat-flow detaches, the front is unstable and the solution flips to a form that is cold throughout the SOL. This corresponds to a 'detached plasma' rather than a 'detached divertor'.

This can be illustrated by Figure 3 where the forms of q_i and q_f are plotted for a sequence of increasing radiation cases. When $q_f(0) > q_i(0)$ (cases 1 and 2) there is a crossing point of q_f and q_i somewhere in the range $0 < z_h < L$ where the front equilibrium Eq. (10) would be satisfied. However, this is unstable, and could never be accessed. Instead, the front will remain at $z_h = 0$. When, as the density is raised (case 3), $q_f(0)$ falls below $q_i(0)$, to cause detachment, there no longer exists an equilibrium, the whole SOL will collapse.

4. Detached Divertors

In view of the above demonstration, it is clear that any steady detached divertor solution requires that κ or H should depend somehow on z_h, so as to stabilize the position of the thermal front by making $dq_f/dz_h > dq_i/dz_h$ at an intersection, $q_f = q_i$.

The generic types of situation that we are most likely to be interested in are illustrated in Figure 4. In Fig. 4(a) is shown a form where a continuous detachment will occur as $q_f(0)$ is lowered below $q_i(0)$, with the front equilibrium moving steadily to larger z_h until the point is reached where the curve of q_f becomes tangent to q_i, beyond which, collapse of the solution (rapid motion of z_h to L) will occur. In Fig. 4(b) is illustrated a shape where a bifurcation will occur as $q_f(0)$ is lowered below $q_i(0)$ and the front will suddenly detach and move to the stable solution point of intersection. Further decrease of q_f will eventually then lead to complete collapse after the tangency point is passed.

Note that q_i has been drawn curved in Fig. 4 to illustrate a case with H decreasing at larger z or, equally well, at larger T. Denoting the mean of H in the inner hot region by $< H >$, one can write $q_i = - < H > (L - z_h)$. The scale length, λ_i, of its variation can be written

$$-\frac{1}{q_i}\frac{dq_i}{dz_h} \equiv \frac{1}{\lambda_i} = \frac{H(z_h)}{< H > (L - z_h)} \quad , \tag{12}$$

if $H(z_h) \approx < H >$, and $L >> z_h$ this is approximately $1/L$.

The q_f variation we require can arise from variation with z_h in any of the quantities S, R or κ. Such variations can be either specific dependency upon z, due, for example, to spatial variation of sources, cross-field transport, neutrals or impurities, or they can be non-local dependence of parameters upon the overall solution. This latter form might encompass deliberate attempts to stabilize the front through feedback, but it also includes naturally occuring effects to do with pressure variation.

It is not obvious how p should be taken to vary with front position. In general, this depends on the density transport problem, which we naturally do not wish to solve here. Perhaps the simplest assumption one could make is that the density at the stagnation point $z = L$ be fixed: n_L. The pressure then depends on the temperature at $z = L$, T_L, and hence on the entire solution in a non-local way. If z_h increases, then clearly T_L decreases, causing $p = n_L T_L$ to decrease, and therefore the radiation to decrease. This leads to a positive slope on q_f, which is a stabilizing effect.

If S is taken constant in the inner hot region, then the value of T_L is the solution of

$$\int_{T_h}^{T_L} \kappa dT = \frac{S}{2}(L - z_h)^2 \quad . \tag{13}$$

For the case of particular interest, where $\kappa = \kappa_1 T^{5/2}$, Spitzer parallel electron conductivity ignoring B-variation, we can obtain an explicit solution

$$T_L = \left[\frac{7S}{4\kappa_1}(L - z_h)^2 + T_h^{7/2}\right]^{2/7} \quad , \tag{14}$$

which is approximately $(7S/4\kappa_1)^{2/7}(L - z_h)^{4/7}$ if $T_L^{7/2} >> T_h^{7/2}$. This leads to a scale length λ_f for q_f

$$\frac{1}{\lambda_f} \equiv -\frac{1}{q_f}\frac{dq_f}{dz_h} = -\frac{1}{p}\frac{dp}{dz_h} = -\frac{1}{T_L}\frac{dT_L}{dz_h} = \frac{4}{7}\frac{1}{L - z_h} \quad . \tag{15}$$

By itself, this gradient is insufficient to stabilize the thermal front, since the scale-length of q_i is shorter, L versus 7L/4.

When we consider, in addition, possible variation in the cross-field heat source S, due, for example, to the proximity to the central plasma, it appears that stabilization of the front is possible. The cross-field heat flux into the whole SOL width is substantially positive when the field line is adjacent to the plasma, i.e. in the main chamber, but zero (or slightly negative) when the field line is adjacent to the cold private flux region, i.e. in the divertor chamber. Therefore, the variation of q_i with z_h in the divertor chamber is small, and the q_i curve has a flat section, from $z_h = 0$ to $z_h = z_x$ where z_x is the position of the x-point, as illustrated in Fig. 5. It is then possible for a stable detached solution to exist, given the q_f slope arising from pressure variation.

The density range over which this stable detachment exists can immediately be deduced from the functional dependence of $q_f \propto p \propto n_L(1 - z_h/L)^{4/7}$. If q_i is constant in the divertor leg ($z_h < z_x$) then as the density is raised, detachment starts when $q_f(0) = q_i$, and the front reaches the x-point when $q_f(0)(1 - z_x/L)^{4/7} = q_i$. The ratio of these two densities is therefore $(1 - z_x/L)^{-4/7}$. Even for a long divertor leg, $z_x/L = 0.3$ say, this ratio is therefore only 1.23, a roughly 20% range in main-chamber density.

The effects of S variation on q_f itself are not as strong as the variation of R, because within the front, the magnitude of R is larger than S by roughly the ratio of

the total length (L) to the front length, a large factor for a well localized front. Spatial dependence of R, would describe a plausible situation in which the impurity fraction (or neutral fraction in the case of hydrogen radiation) possessed an intrinsic gradient along the field-line, for example due to localization in the divertor. Localization near $z = 0$, giving rise to positive dq_f/dz_h (decreasing front radiation as a function of z_h) is stabilizing, requiring a modest scale length of variation of f_I, less than roughly L for stabilization.

The effects of κ variation may be summarized by saying that the front tends to be stabilized when the cold region is in the highest κ region. If the parallel transport is dominant, and given by Spitzer thermal conductivity, then κ-gradients could arise from gradients in Z_{eff} (but not Z_{eff}-gradients arising from the front's temperature dependence, which are not a function of z_h). If impurities are localized to the divertor, then the Z_{eff} gradient should be negative and so this term makes dq_f/dz_h more negative, which is destabilizing.

The variation of κ proportional to $1/B^2$ produces a quite strong intrinsic variation, typically a factor of four in a conventional aspect-ratio tokamak SOL. This will tend to stabilize a front whose cold region is at larger major radius. This introduces a puzzle concerning marfes, whose cold region is on the inboard. It will be resolved in the next section when we consider the additional effects of conductivity asymmetries.

5. Marfes

Two key distinctions between a marfe and a detached divertor are that a marfe consists of two thermal fronts back-to-back which are able to move together, and that the cold region between the fronts, i.e. the marfe itself, is adjacent to the main plasma region.

The mobility of a marfe means that it is unlikely that its stability can depend solely on localization of the radiation sources. This is in contrast to a divertor where localized recycling is a very natural mechanism to localize the radiation effects. The fact that a marfe is next to the main plasma means that it does not experience the stabilizing effect mentioned above for a divertor leg, that the cross-field heat flux, S, might be zero.

The proximity to the main plasma, however, suggests a greater stabilization effect through the density 'feedback'. Again, it is impossible to give a definitive description of how the SOL density might be expected to behave. It is plausible to assume that

the increased density in the marfe tends to diffuse out of the SOL. The simplest model of this overall effect seems to be to assume that, for the marfe case, the *average* density around the poloidal circumference is constant. This would model a situation where the particle cross-field flux divergence into the SOL was proportional to the difference between the local SOL density and some average exterior density. One might note that this assumption of constant average density has been implicitly made in most of the previous linear stability analysis of marfes.

We treat the SOL with a marfe, as a full periodic domain of length 2L. Then, for constant S in the hot region, the solution there for temperature is essentially the same as Eq. (14), namely,

$$T = \left[T_L^{7/2} - \frac{7S}{4\kappa_1}(L-z)^2\right]^{2/7} \quad , \tag{16}$$

while inside the marfe we shall approximate the temperature as constant, T_c. The average SOL density is then

$$\bar{n} = \frac{1}{2L}\int \frac{p}{T}dz = \frac{p}{2L}\left[\frac{2z_h}{T_c} + \int_{z_h}^{2L-z_h}\frac{dz}{T}\right] = p\left[\frac{\zeta}{T_c} + \frac{1}{T_L}\int_\zeta^1 \frac{d\zeta'}{[1-C(1-\zeta')^2]^{2/7}}\right] \quad , \tag{17}$$

where $\zeta = z_h/L$ is the fractional size of the marfe, and $C = 7SL^2/4\kappa_1 T_L^{7/2}$, which is (at most) unity when $T_h^{7/2} << T_L^{7/2}$. The integral over the hot region, the last term, is only slightly underestimated by the simple approximation $(1-\zeta)/T_L$ and this is partially compensated by approximating

$$T_L = [(7SL^2/4\kappa_1)(1-\zeta)^2]^{2/7} \quad . \tag{18}$$

Then the density equation (17) can be solved for pressure, giving

$$p = \frac{\bar{n}T_cT_M}{T_M\zeta + T_c(1-\zeta)^{3/7}} \quad , \tag{19}$$

where $T_M = (7SL^2/4\kappa_1)^{2/7}$ is the maximum temperature in the SOL, i.e. the value of T_L when $\zeta = 0$.

The stabilization implied by this pressure dependence is much stronger than that obtained by the assumption of constant density at $z = L$. Expressed in terms of the scale lengths, the stability of the marfe to expansions or contractions of its size then requires

$$\frac{1}{\lambda_f} = -\frac{1}{pL}\frac{dp}{d\zeta} = \frac{1}{L}\frac{T_M - (3/7)T_c(1-\zeta)^{-2/7}}{T_M\zeta + T_c(1-\zeta)^{3/7}} > \frac{1}{\lambda_i} \approx \frac{1}{L}\frac{1}{1-\zeta} \quad . \tag{20}$$

This may be solved to write the condition on the fractional marfe size as

$$\zeta \lesssim \frac{1}{2}\left[1 - \frac{10}{2^{3/7}7}\frac{T_c}{T_M} - \frac{300}{2^{6/7}343}\left(\frac{T_c}{T_M}\right)^2 + ...\right] \approx \frac{1}{2}\left[1 - 1.1\frac{T_c}{T_M}\right] \quad . \tag{21}$$

Thus, when the average SOL density is kept constant, and the cold temperature is much less than the hot, the marfe size is stable if it is smaller than slightly less than half the poloidal circumference. Experimentally, marfes are observed to be substantially smaller than this, and so are very stable, as far as their size is concerned.

The freedom of the marfe to move around the circumference is not impeded by this density feedback. Instead, its poloidal location must be dictated by asymmetries in κ and possibly S. Experimentally, marfes are always observed on the inboard side of the plasma, although they do tend to be quite mobile. It appears that this inboard preference is caused by finite aspect-ratio effects. It has been proposed that the preference for the inboard is caused by increased cross-field transport at the outboard (in the present approach, larger S there). However, as noted above, there is a strong κ variation with major radius that requires no *ad hoc* assumptions about the spatial variation of anomalous transport. It turns out that this effect causes the marfe to prefer the inboard position, as we now demonstrate.

We assume that the effective conductivity, $\kappa(z,T)$, can be written in a separable form $\kappa = K(z)\kappa(T)$, so that the spatial dependence is contained in the function $K(z)$, which we can choose to be normalized, for example such that $K = 1$ where $B = B_0$. Obviously this separability is possible if Spitzer parallel conductivity dominates. For the purposes of analysing the poloidal asymmetry, it is then best to work in what may be considered 'standard' coordinates. We define new spatial coordinate x and temperature coordinate U by

$$dx = \frac{dz}{K} \quad , \qquad dU = \kappa dT \quad . \tag{22}$$

The transport equation (3) then becomes

$$\frac{d^2U}{dx^2} = -KH \quad . \tag{23}$$

We note that since K is inversely proportional to B^2, it is approximately proportional to the major radius squared. There are then two competing effects. The front dissipation is largest where K is largest, and this makes the marfe tend to move toward the position

of largest K, the outboard. But the effective cross-field transport power, KS, is largest there also, and this tends to move the marfe away from this position. Which of these tendencies is the larger depends on the size of the marfe, as follows.

The motion of either of the thermal fronts is determined, as we analysed above, by the balance between the front dissipation, q_f and the incoming conducted heat q_i. In a marfe, the two fronts are strongly coupled together by the density feedback effect, which adjusts the radiated power in such a way as to maintain essentially constant marfe extent, ζ. Therefore the fronts can move, but must move at the same speed. The speed of motion of a front can be obtained by including the time-dependence of the thermal energy on the right hand side of the conduction equation. That is by replacing H with $H - C_p \partial T/\partial t$, where C_p is the specific heat ($3n$ for two species). Then we can obtain the first integral as before , which may be written in terms of the front speed by assuming that the front retains its shape as it moves:

$$-\frac{dz_h}{dt}\int 2KC_p\frac{\partial T}{\partial z}dT = \int 2KC_p\frac{\partial T}{\partial t}dT = q_i^2 - q_f^2 \quad . \tag{24}$$

This equation applies two each of the two back-to-back fronts. But the sign of the coefficient of dz_h/dt is opposite for the two fronts because their $\partial T/\partial z$ is opposite. We can subtract the two equations corresponding to the right and left fronts (referred to by subscripts + and −) but noting that dz_h/dt is the same for both; they move together. There results

$$I\frac{dz_h}{dt} = (q_{f+}^2 - q_{f-}^2) - (q_{i+}^2 - q_{i-}^2) \quad , \tag{25}$$

where $I = \int_+ - \int_- 2KC_p\partial T/\partial z dT$ is the (positive) effective total resistance to motion of the marfe, due to heat capacity. This equation shows the competing effect of asymmetries in q_f and q_i. The direction of marfe motion is determined by their relative magnitude.

Now the dissipation asymmetry $q_{f+}^2 - q_{f-}^2$ is given simply through $K_+ - K_-$. The heat conduction asymmetry $q_{i+}^2 - q_{i-}^2$ has to be determined by solution of Eq. (23) in the hot region. Although this depends to some extent on the specifics of the geometry under consideration, it proves straightforward to calculate the conduction asymmetry in the approximation that the K-variation can be considered to be given by its lowest Fourier harmonic:

$$K = K_0 + K_1\cos(\pi x/L + \phi) \quad . \tag{26}$$

Naturally, for a circular cross-section tokamak, this can be regarded as an inverse-aspect-ratio expansion. The coefficient is then $K_1/K_0 = 2a/R$, although our result will turn out to be independent of the value of K_1. Taking the marfe to be of negligible extent as far as the external integration is concerned, and located at $x = 0$ we can integrate Eq. (23), with $H = S = \text{const.}$ to obtain

$$q_{i\pm} = -\frac{dU}{dx}|_{\pm} = \frac{SL}{\pi}\left[-\frac{K_1}{K_0}\sin(\phi) \pm \pi\right] \quad . \tag{27}$$

Naturally, the asymmetry depends on ϕ the phase angle (approximately poloidal angle) of the marfe with respect to the K-asymmetry. The value of the asymmetry is

$$q_{i+}^2 - q_{i-}^2 = (SL)^2 \frac{4}{\pi}\frac{K_1}{K_0}\sin\phi \quad . \tag{28}$$

This must be compared with the dissipation asymmetry, which for a marfe of small fractional x-extent, $\xi = (x_+ - x_-)/2L$, is

$$q_{f+}^2 - q_{f-}^2 = q_f^2 \frac{K_1}{K_0}[cos(\phi + \pi\xi) - cos(\phi - \pi\xi)] \approx q_f^2 2\pi \frac{K_1}{K_0}\xi \sin(\phi) \quad . \tag{29}$$

Here, q_f^2 denotes the average of the squared dissipation. The density feedback effect adjusts the pressure so that q_f^2 is equal to the average value of the squared heat inflow, approximately $(SL)^2$. Comparing Eqs. (28) and (29) we see that the stable position of the marfe depends on its fractional extent, ξ. If ξ is small then the conduction asymmetry will be controlling, and the marfe will be located on the inboard. Conversely if the marfe is large the dissipation asymmetry will be larger and the marfe will be on the outboard. Quantitatively, regardless of the magnitude of K_1/K_0, (provided the retention of only lowest Fourier terms is justified) the marfe will be on the inboard if its fractional extent satisfies

$$\xi < \frac{2}{\pi^2} \quad . \tag{30}$$

This rather remarkable result shows that for the extent of experimentally observed marfes (typically 10 to 30 degrees), the finite aspect-ratio asymmetry of the effective conductivity due to geometry is sufficient *alone* to localize the marfe on the inboard. Therefore, even though an increase in S at the outboard side would indeed tend to induce the marfe to occur at the inboard, one cannot deduce from the marfe position the *necessity* of such an asymmetry in the cross-field transport to explain the marfe position, contrary to what is often assumed.

(It should be noted that the compression of the coordinates implied by Eq. (22) and $B_p dz = B_0 dl_p$ means that the x-extent of a specified poloidal angle is larger at the inboard than the outboard. For typical aspect-ratios, in a circular tokamak, the poloidal angle corresponding to an extent of $2/\pi^2$ at the inboard is roughly 20 to 30 degrees but the coordinate transformation depends also on the variation of the poloidal field about which it is hard to generalize.)

Equation (27) is interesting also in respect of the experimentally observed asymmetries of power to the inner and outer divertor plates in single-null divertors. We can regard the single-null divertor configuration as placing the two fronts (in this case the divertor plates) at roughly $\phi = \pi/2$, the top (or bottom) of the tokamak. Then parallel power density ratios as large as approximately $(\pi+1)/(\pi-1) \sim 2$ (outer/inner) may be expected on the basis of effective conductivity asymmetries alone, regardless of any cross-field transport asymmetries. It should be emphasised that these conductivity asymmetries are not in the parallel conductivity *per se*, but in the effective conductivity once the geometric effects of variation in the field angles, the major radius, and the flux-surface spacing have been accounted for. Note, though, that the observed asymmetry at the plates may not reflect the conduction asymmetry (calculated here) directly if radiative losses are important. Also note that the present theory cannot explain the observed dependence of the asymmetry on the direction of $\mathbf{B} \wedge \nabla \mathbf{B}$. So other effects are also significant.

The transition of a detached divertor to a marfe can plausibly be described by a combination of the two types of density behaviour. We assume that the density that is conserved is the average density *in the main chamber*. The rationale for this assumption is that the main-chamber region, adjacent to the bulk plasma, will be influenced by cross-field transport, while the divertor leg density will experience rather independent behaviour dependent on ionization, recycling, and so on. One can readily show, then, that a calculation along the lines of Eqs.(16) through (19) but integrating only over the main chamber region $\zeta_x < \zeta < 1$, leads to

$$\begin{aligned} p &= \bar{n} T_M (1-\zeta)^{4/7} \quad , && \text{for} \quad \zeta < \zeta_x \\ &= \bar{n} T_M \frac{(1-\zeta_x)}{(\zeta-\zeta_x) T_M / T_c + (1-\zeta)^{3/7}} \quad , && \text{for} \quad \zeta > \zeta_x \quad . \end{aligned} \tag{34}$$

Figure 6 shows this combined form. Even though the density range over which the front is confined to the divertor is very narrow, as soon as it emerges into the main

chamber, the much stronger density feedback effect keeps the front close to the x-point. This behaviour bears a remarkable similarity to the experimental observations.

6. Quantitative Radiation Estimates

The strength of what has so far been discussed is that it does not depend on the quantitative details of the radiation process. Nevertheless, it is useful to note that using the present formalism we can immediately transform quantitative assumptions about the radiation function into quantitative predictions about the fronts.

A variety of approximations to the radiation function $Q(T)$ have been used. The variability of these assumptions reflects in part the considerable uncertainty that arises in the radiative processes once finite confinement time and charge-exchange effects [17] are included in the radiation calculations. For carbon a reasonable approximation to the radiation function in coronal equilibrium is

$$Q(T) = 2 \times 10^{-31} (T/10\text{eV})^3 / ((T/10\text{eV})^{4.5} + 1) \quad \text{W m}^3 \quad . \tag{35}$$

However, if the non-coronal effects are dominant, the fall off at higher temperatures is virtually absent, so the exponent in the denominator is reduced to approximately 3. The $q_{\|}$ radiated in the front, assuming Spitzer parallel conductivity, $\kappa_{\|} = \kappa_1 T_e^{5/2}$, is given by

$$q_f^2 = \int \kappa R dT = 2 f_I (nT_e)^2 \kappa_1 \int Q T_e^{1/2} dT_e \quad , \tag{36}$$

where T_e is the temperature in eV. (In calling this q_f we have ignored the distinction between H and R within the front). For the coronal form (Eq. 35) the required integral can be done analytically to any maximum temperature T_m. It is

$$\int_0^{T_m} Q T_e^{1/2} dT_e = \frac{10^{3/2}}{4.5} 2. \times 10^{-31} ln[(T_m/10)^{4.5} + 1] \quad \text{W m}^3 \ (\text{eV})^{3/2} \quad . \tag{37}$$

This is a weak function of the upper temperature T_m. For $T_m = 100$ (eV) it equals 1.5×10^{-29} W m^3 (eV)$^{3/2}$ (and is about 1.0×10^{-31} for $T_m = 50$ eV). This is within a factor of two the same as the value obtained by Lengyel [18] for oxygen. Substituting this value and $\kappa_1 = 2000$ W m^{-1} (eV)$^{-7/2}$ appropriate to $Z_{\text{eff}} = 1$, we get

$$q_f = 3. \times 10^7 f_I^{1/2} \frac{nT}{10^{20} \text{m}^{-3} \text{eV}} \quad \text{W m}^{-2}. \tag{38}$$

This is the amount of parallel heat flow that can be dissipated by a front, as a function of radiative species fraction, f_I, and plasma pressure, nT. As has been noted before

[19], this value tends to be rather lower than is considered necessary for ITER. For example if the SOL pressure is given by $n = 10^{20}$ m^{-3}, $T = 100$ eV, and $f_I = 0.04$, we obtain $q_f = 600$ MW m^{-2}, somewhat less than the roughly 1000 MW m^{-2} peak parallel power density anticipated to flow out of the ITER SOL. However, the actual value of $\int QT^{1/2}dT$ may be larger by up to a factor of 4 if non-coronal effects are strong. This increases the q_f by a factor of 2, which might be sufficient, especially if hydrogen radiation is also important. One can estimate that for atomic hydrogen $\int QT^{1/2}dT \sim 3 \times 10^{-29}$ W m^3 eV$^{3/2}$. However, the atomic fraction, although it may be very large in cold regions, will be a very strong function of position, so the present analysis is not fully satisfactory for hydrogen radiation.

Another parameter that depends on the quantitative form of the radiation function is the expected size of the marfe. This size is determined by the assumptions about density. But if we assume that the average density after the marfe has formed is the same as in the approximately uniform state prior to the marfe formation, an estimate can be obtained.

When the marfe is formed, the large fractional decrease in its temperature causes a strong increase in its local density at constant pressure; (this is the "condensation" effect). If the marfe extent were a substantial fraction of the periphery, then the pressure would have to drop a lot in order to conserve average density, as given by Eq. (19). However the pressure cannot drop too much because if it did the radiation would be insufficient to sustain the thermal front and the marfe would shrink. So instead, the marfe adjusts its size (downward) till the pressure is high enough to sustain the front.

The condition for total power balance can be written by forming the first integral over the half SOL (ignoring in this estimate the complication of asymmetries)

$$f_I p^2 \kappa_1 \int_{T_c}^{T_L} QT^{1/2}dT = \int \kappa R dT = \int \kappa S dT \quad . \tag{39}$$

We now need to estimate the lower limit of p allowed by this expression. This is given by the lower limit of S (relative to radiation). The estimate may be obtained by considering the linear stability of the uniform state prior to marfe formation. The condition for this state to be unstable to marfe formation of the lowest order mode (m=1) is

$$f_I p^2 \frac{d}{dT}\left(\frac{Q}{T^2}\right) - \frac{dS}{dT} + \kappa\left(\frac{\pi}{L}\right) < 0 \quad . \tag{40}$$

The stability of this state to a symmetric (m=0) collapse, which occurs at constant density, rather than constant pressure, is

$$f_I n^2 \frac{dQ}{dT} - \frac{dS}{dT} \geq 0 \quad . \tag{41}$$

Both of these stability criteria must be applied at the equilibrium, which statisfies:

$$f_I n^2 Q_i = S \quad . \tag{42}$$

(Q_i denotes the initial equilibrium value). Whether or not a marfe instability will occur, by virtue of satisfying Eq. (40), *before* the entire SOL collapses because of violating Eq. (41) depends on the relative importance of the additional conductivity term in Eq. (40). We will simply assume that conduction is low enough that a marfe does form. If so, then the collapse stability equation (41) still dictates the minimum value of S that must be used in Eq. (39). Therefore, we will use the marginal collapse stability criterion in our estimate.

To make quantitative progress we need to adopt some specific functional form for $S(T)$. We shall use

$$S(T) = \frac{S_0}{T_s}(T_s - T) \quad , \tag{43}$$

which represents a plausible approximation to cross-field transport under which an equilibrium would be reached in the absence of radiation at temperature T_s. If we take, for generality, the logarithmic derivative of Q to be $-C$:

$$\frac{dQ}{dT} = -C\frac{Q}{T} \quad , \tag{44}$$

then we can solve the simultaneous equilibrium and marginal stability (equality in Eq. (41)) to get $T_i = T_s C/(1+C)$ for the equilibrium temperature, and in particular

$$S_0 = (1+C) f_I \bar{n}^2 Q_i \quad . \tag{45}$$

We substitute this into Eq. (39) and after elementary integration and some rearrangement we get

$$\frac{\bar{n}}{p} = \frac{1}{T_L}\left[\frac{7}{2(1+C)}\right]^{1/2}\left[\frac{\int Q T^{1/2} dT}{Q_i T_L^{3/2}}\right]^{1/2} \frac{1}{(1-\frac{7}{9}\frac{T_L}{T_s})^{1/2}} \quad . \tag{46}$$

Evaluating this expression using the carbon radiation form, Eq. (35), for which $C \approx 1.5$ and dispensing with a factor $(T_M/T_L)(T_L/T_i)(1 - 7T_L/9T_s)^{-1/2}$, which is nearly unity in most cases, we get $\bar{n}T_M/p \approx 1.5$.

The equation (19) for p in terms of ζ can be approximately solved for ζ in terms of p as

$$\zeta = \frac{\bar{n}T_M/p - 1}{T_M/T_c - 3/7} \quad , \tag{47}$$

which then yields on substitution of $\bar{n}T_M/p$ and ignoring $3/7$ in comparison to T_M/T_c:

$$\zeta \approx 0.5\frac{T_c}{T_M} \quad . \tag{48}$$

For typical radiation functions, the cold temperature T_c, at which the marfe will equilibrate because of falling radiation, is a few eV. So a typical value of T_c/T_M is perhaps 0.1. We therefore predict that the marfe extent is quite small, 5% of the poloidal perimeter. Clearly, the exact value of $\bar{n}T_M/p$ depends on the shape of the radiation function, as represented by the value of C and the Q factors in Eq. (46). Nevertheless, the dominant effect that causes the marfe to be small is the small value of T_c/T_M, which is a robust feature of the radiation function.

7. Summary

By nonlinear analysis of the parallel heat transport equation combined with pressure balance, and making reasonable assumptions about density control, we have demonstrated that a variety of qualitative and quantitative features of thermal fronts in tokamak scrape-off-layers can be understood.

Divertor detachment has been shown to be possible either through a bifurcation or through continuous detachment, in either case requiring either localization of radiating species to the divertor or, more naturally perhaps, density control to stabilize the front to the divertor. Such mechanisms are almost certainly already in play in the experiments. Plausible assumptions about the density behaviour suggest that detachment may be continuous but that the range of densities over which the front remains in the divertor leg is small ($\sim$ 20%). The anticipated transition to much stronger density feedback effects as the front emerges into the main chamber causes the resulting marfe to remain localized to the x-point over a much larger density range.

Analysis of non-divertor marfes has explained in a very natural way several characteristic features. A marfe's robust identity as a cold region of essentially constant

size has been shown to be a consequence of the conservation of average density in the SOL, which strongly stabilizes the marfe size, provided it is small. The marfe's position on the inboard of the torus has been shown to be a natural (though somewhat subtle) consequence of the purely geometric effects on parallel heat flow, regardless of any presumed asymmetries in cross-field transport, again provided its fractional extent is small. The expected fractional size of a marfe has been estimated to be of order the ratio of the cold to the hot temperatures, under conditions of density conservation.

Undoubtedly there are many important effects that are omitted from the present analysis, notably the transport dynamics of neutral hydrogen. Nevertheless, the features we have deduced are in good agreement with experimental observations.

Acknowledgements

I would like to thank the JET Joint Undertaking for their hospitality during the writing of this paper. The work was supported by US Department of Energy contract No DE-AC02-78ET5103.

References

[1] PETRIE, T.P., et al., J. Nucl. Mater. **196-198** (1992) 848.

[2] JANESCHITZ, G., et al., in Controlled Fusion and Plasma Physics (Proc. 19th European Conference Innsbruck, 1992) Vol 16C, Part II, European Physical Society, Petit-Nancy, Switerland (1992) 727.

[3] HUTCHINSON, I.H., et al., Phys. Plasmas, **1** (1994) 1511.

[4] LIPSCHULTZ, B., J. Nucl. Mater. **145-147** (1987) 15.

[5] HOSOGANE, N., et al., J. Nucl. Mater. **196-198** (1992) 750.

[6] MERTENS, V., et al., in Controlled Fusion and Plasma Physics (Proc. 20th European Conference Lisbon, 1993) Vol 17C, Part I, European Physical Society, Petit-Nancy, Switerland (1993) 267.

[7] SCHNEIDER, R., et al., J. Nucl. Mater. **196-198** (1992) 811.

[8] ROGNLIEN, T.D., et al., J. Nucl. Mater. **196-198** (1992) 346.

[9] KASTELEWICZ, H., et al., in Controlled Fusion and Plasma Physics (Proc. 20th European Conference Lisbon, 1993) Vol 17C, Part II, European Physical Society, Petit-Nancy, Switerland (1993) 807.

[10] STOTLER, D.P., et al., J. Nucl. Mater. **196-198** (1992) 894.

[11] HUTCHINSON, I.H., Phys. Rev. A **37** (1988) 4358.

[12] NEUHAUSER, J., SCHNEIDER, W., and WUNDERLICH, R., Nucl. Fusion (1986) 1679.

[13] DRAKE, J.F., Phys. Fluids **30** (1987) 2429.

[14] WESSON, J.A., and HENDER, T.C. Nucl. Fusion **33** (1993) 1019.

[15] KAW, P.K., DESHPANDE, S., AVINASH, K., and RATH, S., Phys. Rev. Lett. **65** (1990) 2873.

[16] CAPES, H., GENDRIH, PH., and SAMAIN A., Phys. Fluids **B4** (1992) 1287.

[17] CAROLAN, P.G., and PIOTROWICZ, V.A., Plasma Phys. **25** (1983) 1065.

[18] LENGYEL, L.L., Analysis of Radiating Plasma Boundary Layers, report IPP 1/191, (1981) IPP, Garching.

[19] NEUHAUSER, J., IPP Garching, private communication (1993).

Figures

Fig 1. Illustrative functional form of source terms versus temperature. Cross-field flux (S), radiation (R), and total (H).

Fig 2. A thermal front solution of the equation $d/dz(\kappa dT/dz) = -H$, showing the 'cold', 'thermal front', and 'hot' regions. (This is actually a numerical solution using the forms of Fig. 1 and $\kappa \propto T^{5/2}$, but with an additional spatially dependent factor proportional to $\exp[-(z/0.13L)^2]$ multiplying R to stabilize the front's position. See text.)

Fig 3. Spatial variation of the heat flux at the front, q_i, and the front's dissipation, q_f, as a function of front position, for a uniform SOL and increasing values of density (cases 1 to 3).

Fig 4. Schematic forms of power flux variation that would lead to continuous detachment (a), and bifurcation (b).

Fig 5. Form of q_i appropriate for a uniformly heated SOL except that the region $0 \leq z/L \leq 0.2$ corresponds to the divertor leg where the cross-field transport is negligible. The form of $q_f \propto (1 - z_h/L)^{4/7}$ appropriate to the density feedback effect with constant stagnation-point density is shown. Stable detachment can be obtained, but over a narrow density range.

Fig 6. Power flux forms for a divertor plasma with a transition to marfe density behaviour for fronts in the main chamber. There is a strong tendency for the front to be near the x-point.

Fig 1

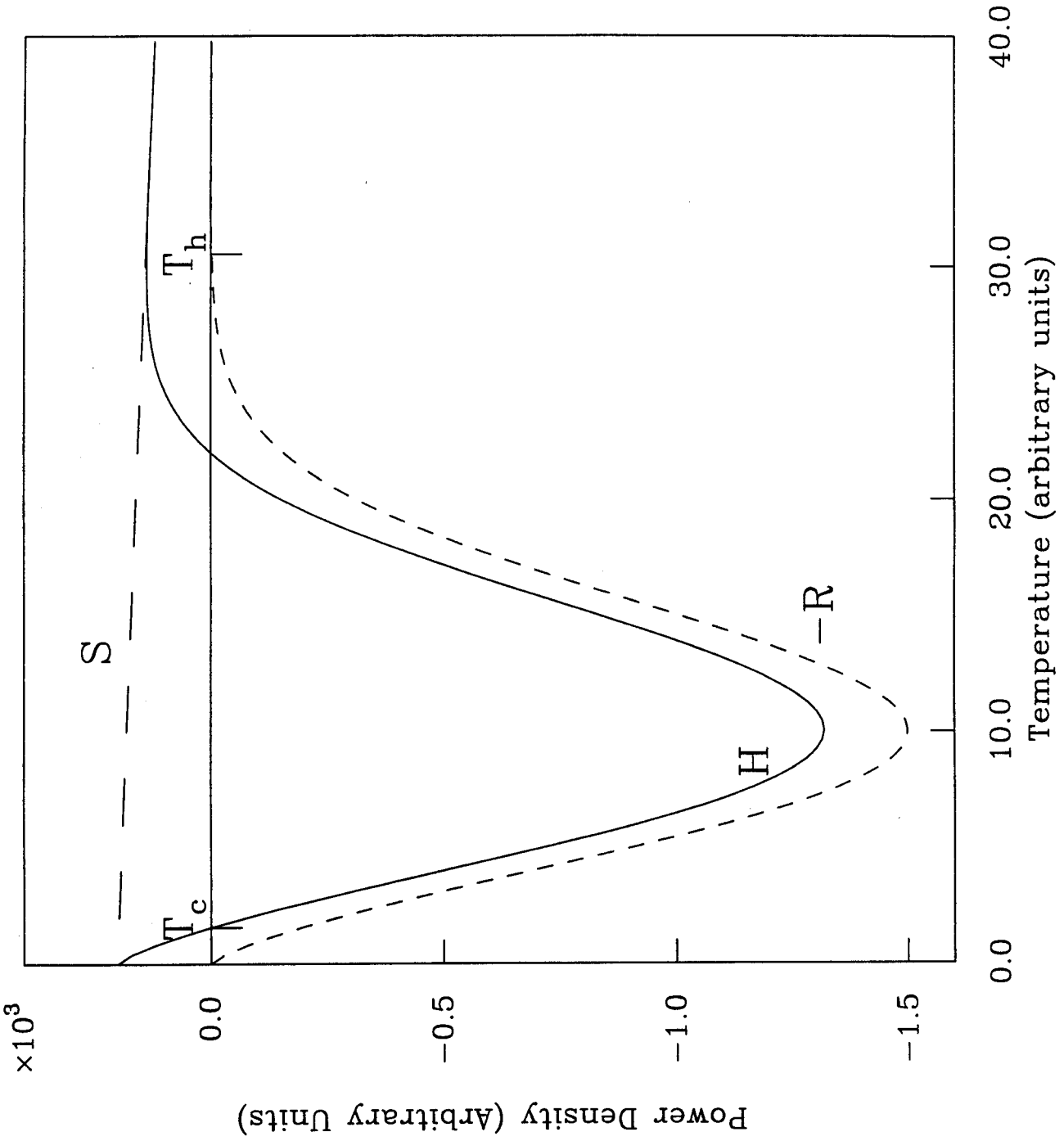
Power Density (Arbitrary Units)
×10^3
0.0
−0.5
−1.0
−1.5
0.0
10.0
20.0
30.0
40.0
Temperature (arbitrary units)
S
R
H
T_h
T_c

Fig 2

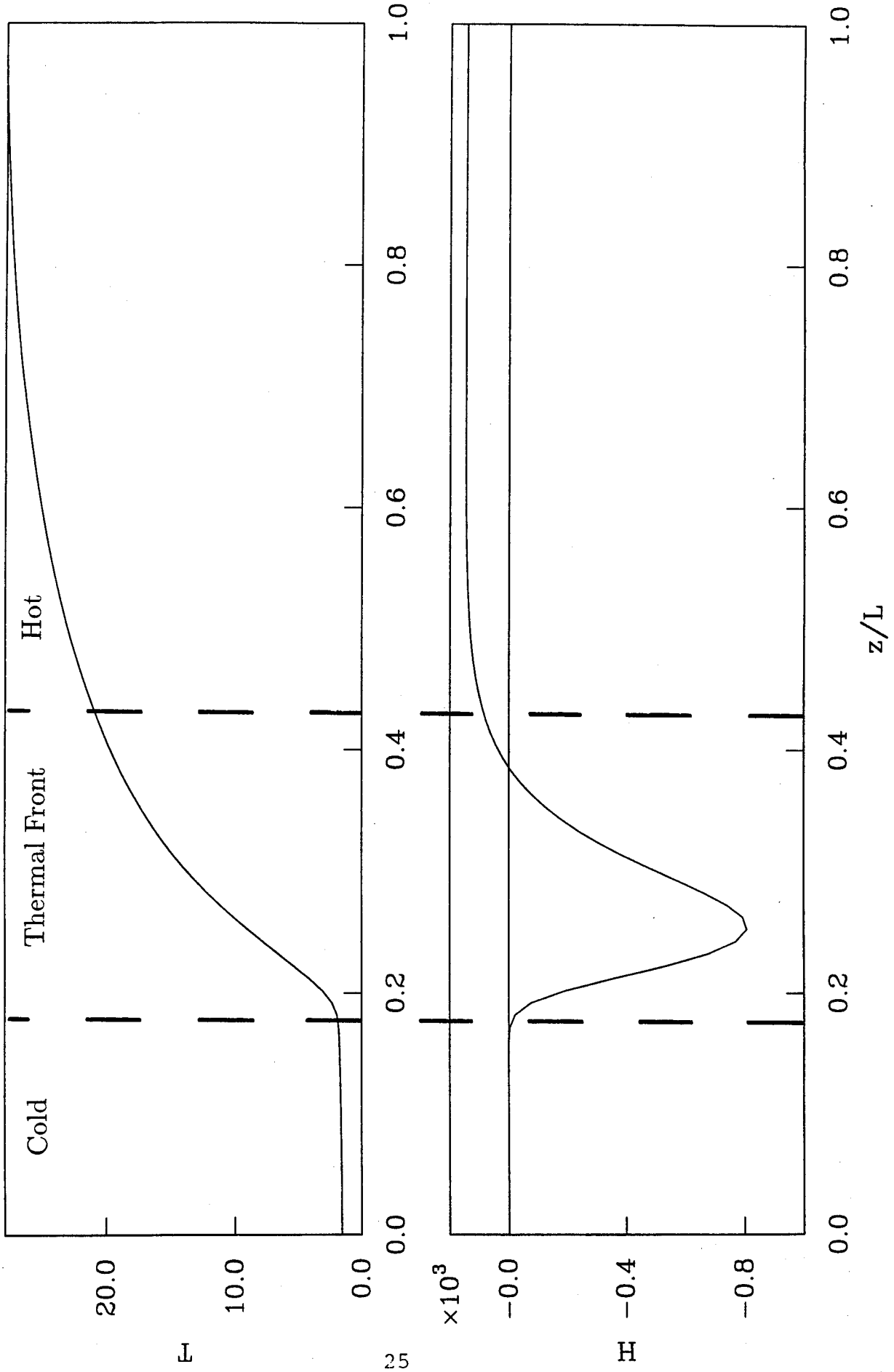
Cold
Thermal Front
Hot
T
20.0
10.0
0.0
H
×10³
−0.0
−0.4
−0.8
0.0
0.2
0.4
0.6
0.8
1.0
z/L

Fig 3

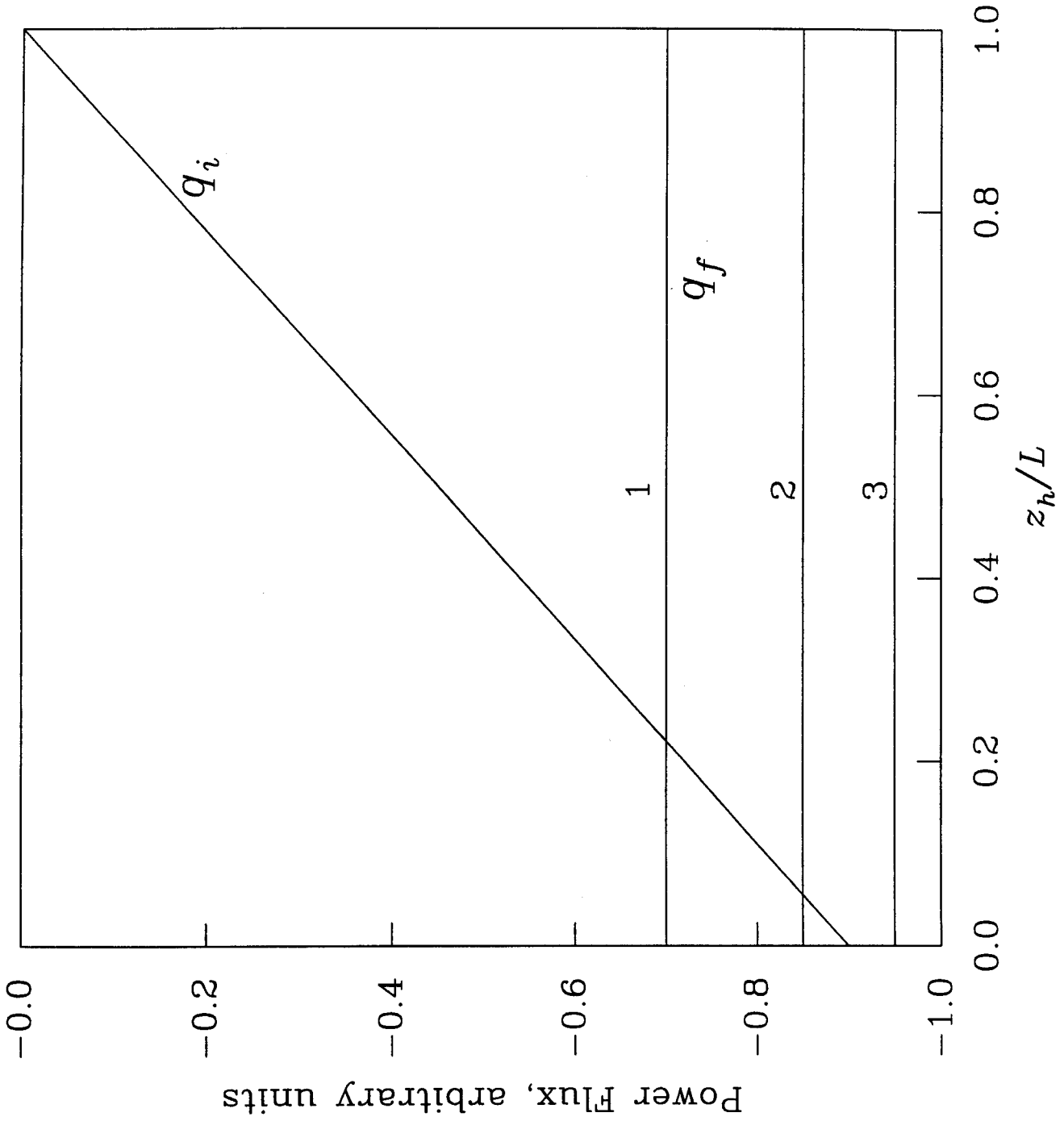
Power Flux, arbitrary units
−0.0
−0.2
−0.4
−0.6
−0.8
−1.0
0.0
0.2
0.4
0.6
0.8
1.0
z_h/L
q_i
q_f
1
2
3

Fig 4.

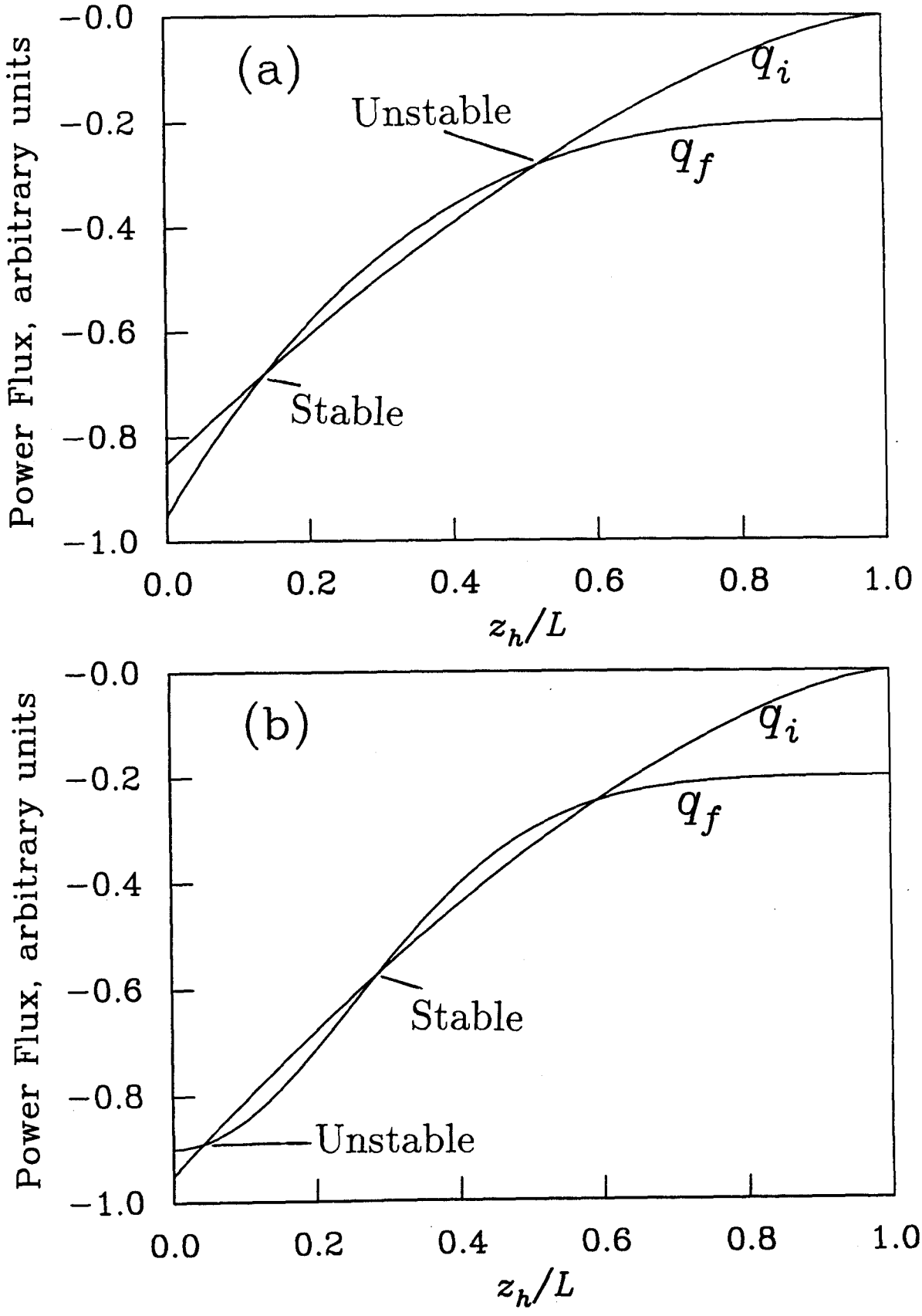
(a)
Unstable
Stable
q_i
q_f
Power Flux, arbitrary units
−0.0
−0.2
−0.4
−0.6
−0.8
−1.0
0.0
0.2
0.4
0.6
0.8
1.0
z_h/L
(b)
Stable
Unstable
q_i
q_f
Power Flux, arbitrary units
−0.0
−0.2
−0.4
−0.6
−0.8
−1.0
0.0
0.2
0.4
0.6
0.8
1.0
z_h/L

Fig 5

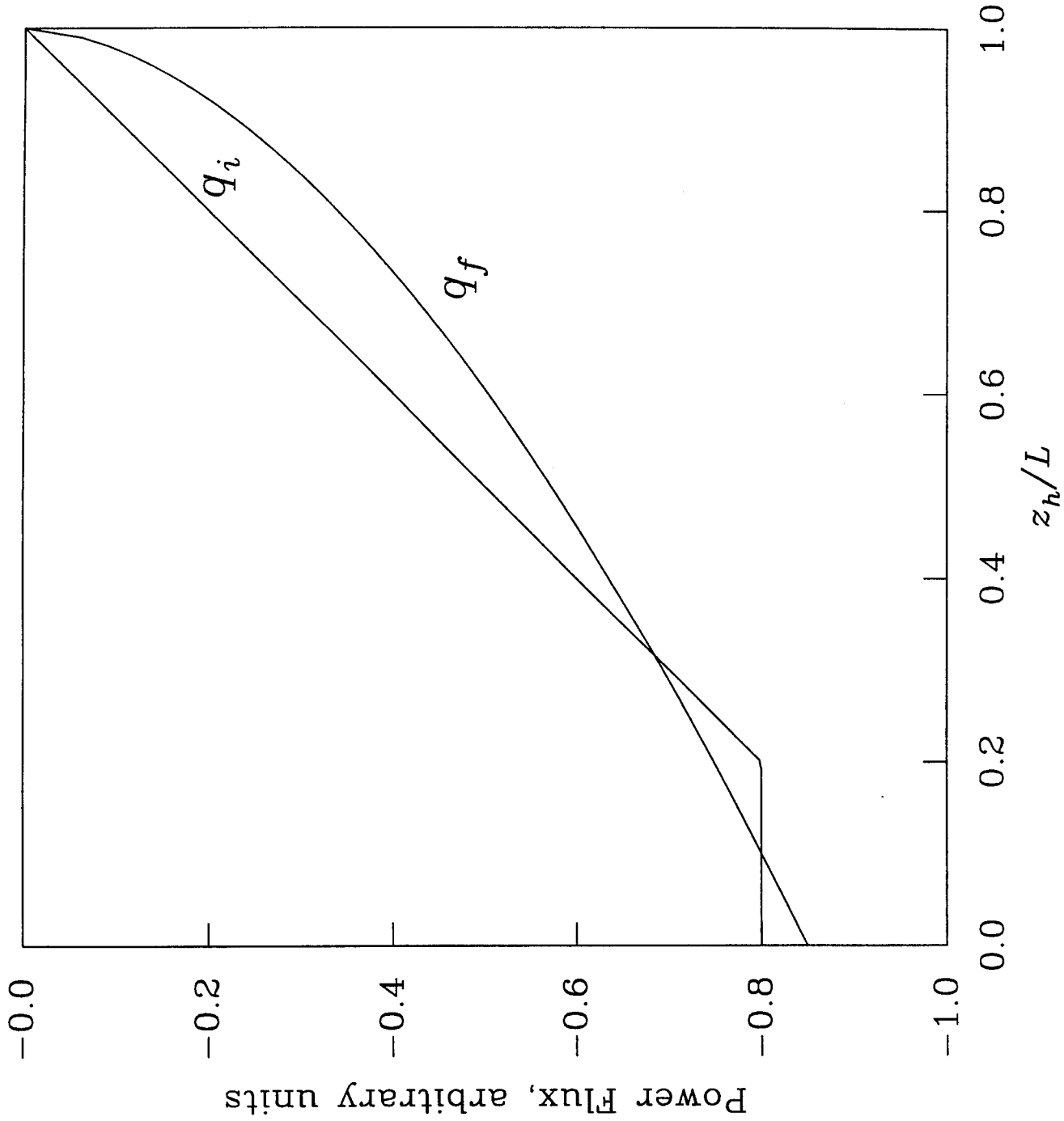
q_i
q_f
Power Flux, arbitrary units
−0.0
−0.2
−0.4
−0.6
−0.8
−1.0
0.0
0.2
0.4
0.6
0.8
1.0
z_h/L

Fig 6

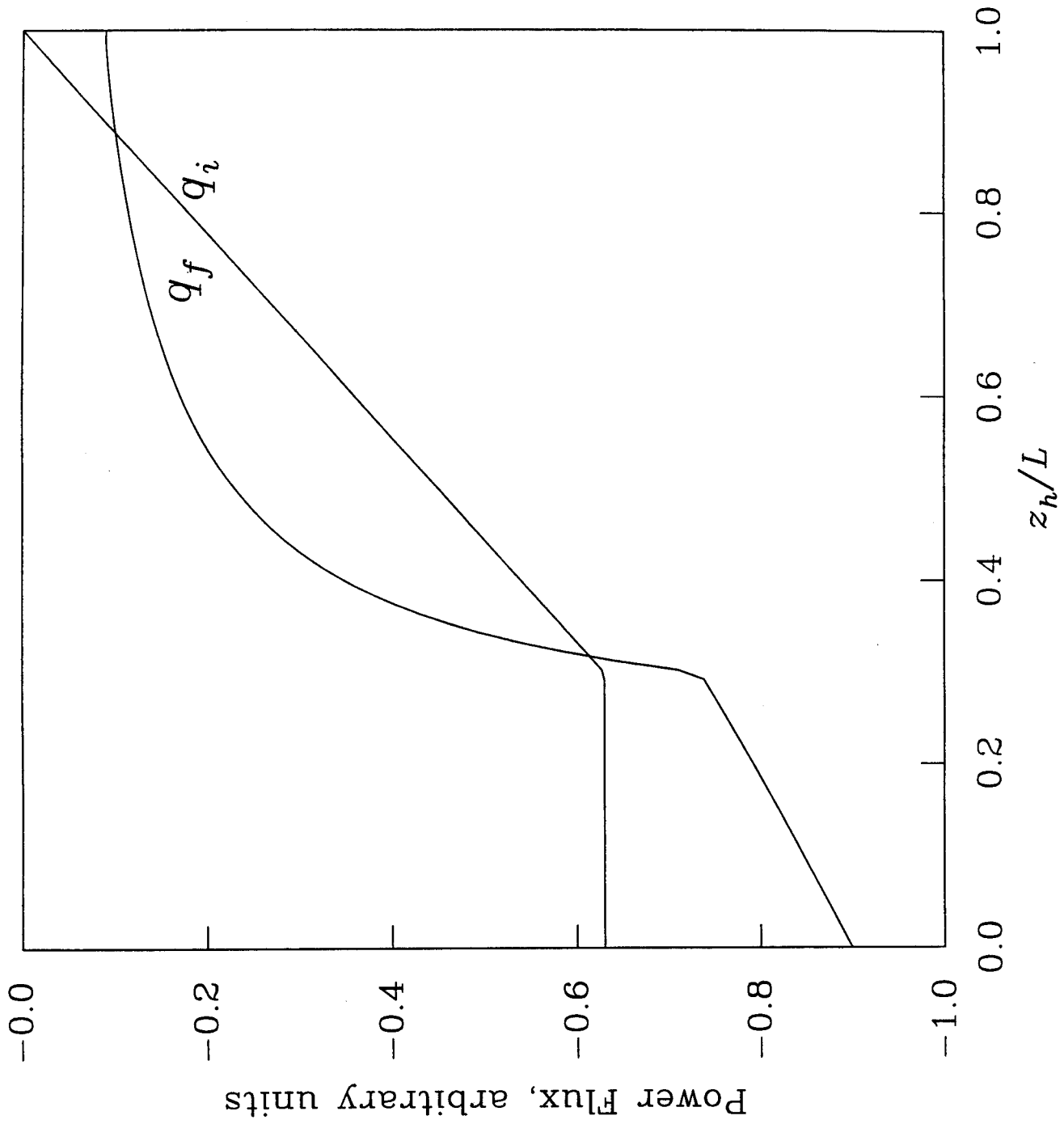
q_i
q_f
Power Flux, arbitrary units
−0.0
−0.2
−0.4
−0.6
−0.8
−1.0
0.0
0.2
0.4
0.6
0.8
1.0
z_h/L